Published in final edited form as:
J Mol Biol. 2008 May 16; 378(5): 1074–1083. doi:10.1016/j.jmb.2008.03.040.

Porphyrin Binding and Distortion and Substrate Specificity in the Ferrochelatase Reaction: The Role of Active Site Residues

Tobias Karlberg[1], **Mattias D. Hansson**[2], **Raymond K. Yengo**[1], **Renzo Johansson**[1], **Hege O. Thorvaldsen**[1], **Gloria C. Ferreira**[3,4], **Mats Hansson**[2], and **Salam Al-Karadaghi**[1,*]

[1]Department of Molecular Biophysics, Centre for Molecular Protein Science, Lund University, P.O. Box 124, SE-22100 Lund, Sweden

[2]Department of Biochemistry, Centre for Molecular Protein Science, Lund University, P.O. Box 124, SE-22100 Lund, Sweden

[3]Department of Molecular Medicine, College of Medicine, University of South Florida, Tampa, FL 33612-4799, USA

[4]H. Lee Moffitt Cancer Center and Research Institute, University of South Florida, Tampa, FL 33612-4799, USA

Abstract

The specific insertion of a divalent metal ion into tetrapyrrole macrocycles is catalyzed by a group of enzymes called chelatases. Distortion of the tetrapyrrole has been proposed to be an important component of the mechanism of metallation. We present the structures of two different inhibitor complexes: (1) *N*-methylmesoporphyrin (*N*-MeMP) with the His183Ala variant of *Bacillus subtilis* ferrochelatase; (2) the wild-type form of the same enzyme with deuteroporphyrin IX 2,4-disulfonic acid dihydrochloride (dSDP). Analysis of the structures showed that only one *N*-MeMP isomer out of the eight possible was bound to the protein and it was different from the isomer that was earlier found to bind to the wild-type enzyme. A comparison of the distortion of this porphyrin with other porphyrin complexes of ferrochelatase and a catalytic antibody with ferrochelatase activity using normal-coordinate structural decomposition reveals that certain types of distortion are predominant in all these complexes. On the other hand, dSDP, which binds closer to the protein surface compared to *N*-MeMP, does not undergo any distortion upon binding to the protein, underscoring that the position of the porphyrin within the active site pocket is crucial for generating the distortion required for metal insertion. In addition, in contrast to the wild-type enzyme, Cu^{2+}-soaking of the His183Ala variant complex did not show any traces of porphyrin metallation. Collectively, these results provide new insights into the role of the active site residues of ferrochelatase in controlling stereospecificity, distortion and metallation.

Keywords

iron; heme synthesis; substrate distortion; catalysis; metallation

*Corresponding author. salam.al-karadaghi@mbfys.lu.se.

Introduction

Metallated tetrapyrroles are required in a wide range of biological processes such as photosynthesis, oxygen transport, respiration, drug metabolism and enzymatic oxidation.[1] In biological systems, the insertion of specific divalent metal ions into tetrapyrroles is catalyzed by a group of enzymes called chelatases. The best characterized among these are protoporphyrin IX ferrochelatase, the terminal enzyme of heme biosynthesis that catalyzes the insertion of Fe^{2+} into protoporphyrin IX (ppIX), as well as magnesium and cobalt chelatases, which catalyze divalent metal ion insertion in the chlorophyll and vitamin B_{12} biosynthetic pathways, respectively.[2–5] The mechanism of the porphyrin metallation reaction has been under scrutiny by organic chemists and enzymologists for more than three decades.[6] Among the tenets held for the mechanism of catalysis is distortion of the tetrapyrrole macrocycle so as to expose the lone-pair orbitals of the pyrrole nitrogen atoms to the incoming metal ion and facilitate formation of the first metal–nitrogen bond.[2,3,7] Additional factors may include the type of distortion of the macrocycle, which may be specific for different metals, acceleration of the rate of ligand exchange between the protein and the porphyrin, and control of specificity of the reaction by dedicated metal chaperones that deliver the metal ion to the chelatase. Frataxin is one such factor; it has been shown to support the ferrochelatase reaction through iron delivery and direct interaction with the enzyme.[8–11]

In enzymatic reactions, distortion of the macrocycle is believed to happen upon binding of the tetrapyrrole to the active site of the enzyme. This has been suggested by the results of several studies, one of which was the study of porphyrin binding to murine ferrochelatase using resonance Raman (RR) spectroscopy.[12,13] This showed that the saddling deformation was the dominating distortion in planarity. Later, it was shown that mutant variants of the murine ferrochelatase with weakened induction of the saddled distortion had reduced catalytic efficiency as compared to that of the wild-type enzyme. In addition, alterations in the vibrational modes associated with the porphyrin vinyl and propionate groups were observed, suggesting that reorientation and relocation of the macrocycle can occur in protein with mutated active site residues.14 RR experiments also demonstrated that ferrochelatase and a catalytic antibody, known to catalyze porphyrin metallation, induced different types of distortion, while the activation of the Raman band describing the out-of-plane vibration was related directly to the degree of affinity maturation of the antibody.15,[16] These results clearly suggest that, to a great extent, it is the environment of the active site that controls the orientation and distortion of the porphyrin.

X-ray crystallographic studies of ferrochetalase from *Bacillus subtilis*,[17] man[18] and *Saccharomyces cerevisiae*,[19] and the subsequently determined complexes with inhibitor and substrate revealed valuable details of porphyrin binding and interaction with the protein, and suggested a mechanism for macrocycle distortion. Thus, the structure of the complex of *B. subtilis* ferrochelatase with the potent inhibitor *N*-methylmesoporphyrin (*N*-MeMP)[20] demonstrated that the enzyme caused additional distortion of the porphyrin, which is normally distorted in solution due to the presence of the methyl group. This additional distortion was mainly of a saddled-ruffled type. Moreover, only one isomer in which pyrrole ring A was *N*-alkylated (regio-isomer N_A) was bound in the active site pocket, showing that only a certain type of distortion could be accommodated by the binding pocket. Interestingly, a similar type of distortion was found in mesoporphyrin bound to a catalytic antibody capable of catalyzing porphyrin metallation, and which was generated against *N*-MeMP.[21] The recently published X-ray structures of the Glu343Lys variant of human ferrochelatase in complex with ppIX, of the lead-inhibited intermediate of the wild-type enzyme, and of the Phe110Ala variant in complex with product (heme) have shown that the porphyrin is rotated by about 100° and buried by an additional 4.5 Å deeper into the active site cleft as compared to the position of *N*-MeMP in *B. subtilis* enzyme.[22,23] These differences in porphyrin binding and the apparent differences

in the structures of the porphyrin binding pockets of the catalytic antibody and ferrochelatase clearly suggest that the distortions required for the metallation reaction may be imposed by different environments of the substrate.

We present the structures of two different inhibitor complexes: (1) the His183Ala variant of *B. subtilis* ferrochelatase with *N*-MeMP; and (2) the wild-type enzyme with deuteroporphyrin IX 2,4-disulfonic acid dihydrochloride (dSDP, Fig. 1). While dSDP is a weak inhibitor of bovine and murine ferrochelatases with K_i and k_d in the micromolar range, *N*-methylprotoporphyrin IX (*N*-MePP) has K_i and k_d in the nanomolar range.[24–26] The structure of the complex with dSDP reveals for the first time the mechanism of inhibition of ferrochelatase by inhibitors with bulky substituents at positions 2 and 4 of the porphyrin ring. His183 is one of the few invariant residues in the ferrochelatase family. It has been implicated in metal binding, proton extraction and interactions with the porphyrin.[27–32] Here, we show that His183 also contributes to control the type of porphyrin distortion and that it is indispensable for porphyrin metallation.

Results

Structure of the His183Ala:*N*-MeMP complex of ferrochelatase

The crystals of the His183Ala variant of ferrochelatase in complex with *N*-MeMP diffracted to a resolution of 2.4 Å, with overall three-dimensional structure similar to that observed for the complex of the wild-type enzyme with the same inhibitor.[20] The porphyrin binds with rings A and B positioned inside the previously identified porphyrin-binding cleft, located between the two domains of the protein. Pyrrole rings C and D, which carry the acidic propionate side chains, point towards the solvent. The loop between helices 1 and 2 (residues 19–49) moves away from its position in the porphyrin-free structure by about 2.4 Å, while helix 2 moves towards the porphyrin by about 1.8 Å (Fig. 2a). Also, the loop between residues 224 and 233 in domain II changes its conformation slightly to avoid a steric clash with the porphyrin. One of the largest displacements involves the side chains of residues Tyr26, Leu43 and Phe120. Tyr26 and Phe120 move by 7 Å and 2.5 Å, respectively, which avoids a steric clash with the porphyrin, while Leu43 moves by about 2.2 Å away from the new position of Tyr26 (Fig. 2a). Interestingly, in the complex with dSDP (see below) these residues are displaced in a similar fashion, although in this case the inhibitor does not penetrate the binding cleft to the same extent as *N*-MeMP. On the other hand, helices 1 and 2, and the loop between them, when compared to the wild-type protein, are not displaced in the dSDP complex.

A surprising feature of the complex of *N*-MeMP and the His183Ala variant of ferrochelatase, as compared to the complex with the wild-type enzyme, is that a different isomer of *N*-MeMP binds in the active site pocket. In the chemical synthesis of commercially available *N*-MeMP, methylation of each of the four pyrrolenine nitrogen atoms can occur from both sides of the ring, giving rise to eight different isomers with eight different out-of-plane distortions of the pyrrole ring. A presentation of the structures of the isomers that bind to the wild-type enzyme and to the His183Ala variant is given in Fig. 1. While wild-type ferrochelatase binds an *N*-MeMP isomer with methylated pyrrole ring A (regio-isomer N_A), the His183Ala variant binds an isomer in which ring B is methylated (regio-isomer N_B). The distorted pyrrole is still facing the space between Glu264 and Ala183 (Fig. 2a), where metals were found to bind in metal complexes of *B. subtilis* ferrochelatase.[30,32] A superposition of the structures of wild-type and His183Ala mutant complexes with *N*-MeMP (not shown in the figure) shows that the ethyl group on pyrrole ring B would make too close a contact with the imidazole group of His183 (around 2 Å), which explains why this isomer is not favored by the wild-type enzyme.

Porphyrin distortion

Distortion of the macrocycle has been suggested to be one of the factors that may control the chemical properties of porphyrins in living organisms.[33,34] Normally planar in solution, porphyrin groups may be distorted from planarity upon binding to proteins as a result of the asymmetric environment and interactions with main- and side-chain atoms.[35] To describe these distortions, the method of normal-coordinate structural decomposition (NSD) has been developed.[36] NSD may be used to decompose the total out-of-plane distortion of a porphyrin structure into ruffling (*B1u*), saddling (*B2u*), waving (*Egx* and *Egy*), doming (*A2u*) and propellering (*A1u*) deformations.[34] Using the NSD web server†, we calculated the type and magnitude of the deformations that contribute to the total distortion of *N*-MeMP bound to wild-type ferrochetalase and the His183Ala variant. The NSD calculations (Fig. 3) show that saddling is the largest planarity distortion of *N*-MeMP bound to either wild-type ferrochelatase or mutant protein. This is in agreement with earlier spectroscopic observations.[12,13] However, the distortion is clearly more pronounced in the complex with the His183Ala protein (−1.41 Å compared to −0.958 Å for the wild-type enzyme). The two structures have approximately the same degree of ruffling, but for the inhibitor bound to wild-type protein doming is around half of that of the His183Ala variant-bound inhibitor. Finally, the analysis shows that *x*-waving is predominant in the complex with wild-type ferrochelatase, while *y*-waving is predominant in the porphyrin bound to the His183Ala enzyme. In neither case does the propellering deformation contribute significantly to distortion. It can also be seen from Fig. 3 that the saddling distortion is almost absent from the porphyrin in solution. We have also compared the distortions imposed on *N*-MeMP and mesoporphyrin by the catalytic antibody to the distortions imposed by ferrochelatase. Although in both cases the regio-isomer N_A of *N*-MeMP is bound, in the case of the antibody a different enantiomer is bound, with the methyl group directed to the opposite side of the macrocycle plane as compared to the enantiomer bound to ferrochelatase. This is reflected in the opposite sign of the deformations in ferrochelatase and the antibody. As seen from the figure, the absolute values of the various displacements of *N*-MeMP bound to the catalytic antibody and wild-type ferrochelatase are largely the same with the exception of ruffling, which for the ferrochelatase complex is twice that of the antibody. On the other hand, mesoporphyrin has much higher ruffling (−1.1947 Å) and *y*-waving (0.6472 Å), as compared to *N*-MeMP (−0.2589 Å and −0.0.1286 Å, respectively).

Metal soaking of the complex of *N*-MeMP and the His183Ala variant of ferrochelatase

Crystals of the *N*-MeMP:His183Ala variant complex diffracted to 1.5 Å resolution. Examination of the electron density maps calculated with F_o-F_c coefficients did not show any traces of bound metal. This is in contrast to earlier soaking experiments, which showed gradual accumulation of metal in the centre of the macrocycle and demethylation of *N*-MeMP.[31] The absence of metal was also evident from the high resolution of the data, since in all previous metal soaking experiments incorporation of the metal into the porphyrin had resulted in deterioration of the resolution and quality of the X-ray data. These results provide the most direct evidence of the crucial role of the invariant His183 in the metallation reaction and clearly suggest that the metal must enter into the ring from the side that faces His183. Earlier work demonstrated that the His183Ala variant of *B. subtilis* ferrochelatase did not have any catalytic activity when assayed with the substrate ppIX. In addition, metal soaking of the porphyrin-free crystals of this protein did show any traces of metal bound close to Ala183.[32] Together, these results suggest that metal insertion into of *N*-MeMP and the substrate ppIX follow a similar path.

†http://jasheln.unm.edu/jasheln/content/nsd/nsd__welcome.htm

Structure of the dSDP complex with ferrochelatase

In a study of the effect of the size of substituents at positions 2 and 4 of the porphyrin ring on binding to ferrochelatase, it was concluded that molecules with large substituents, such as in *OO′*-diacetylhematoporphyrin, 2,4-bis-acetal-deuteroporphyrin, 2,4-bis-glycol-deuteroporphyrin and dSDP, inhibit ferrochelatase with similar K_i values—which were in the micromolar range.[37] In the case of dSDP k_d assayed with the mouse ferrochelatase was 0.33 μM.[25] Approximately the same k_d value was obtained by us for wild-type *B. subtilis* ferrochelatase, 0.32±0.18 μM. We crystallized dSDP in complex with wild-type *B. subtilis* ferrochelatase and data were collected to 1.8 Å resolution. The overall conformation of the complex is close to that of the wild-type ferrochelatase, with the exception of the displacement of the side chains of the above-mentioned residues Tyr26, Leu43 and Phe120.

The inhibitor binds close to the surface of the protein, with one of the disulphonic acid groups in close contact with the side chain of His183 and the hydroxyl group of Tyr13 (3.2 Å and 2.7 Å, respectively) (Fig. 4a). The second disulphonic acid group interacts with the guanido group of Arg30 and the main-chain amide group of Asn225 (3.0 Å). Further stabilization is achieved through interactions of the backbone oxygen of Ile29 with one of the pyrrole-nine nitrogen atoms, and one of the propionate groups with the guanido group of Arg33. In addition, there are hydrophobic interactions with Ile29, Phe120, Gly224, Thr226 and Trp230. These interactions trap the porphyrin approximately halfway into the binding cleft, as compared to the binding of *N*-MeMP, although the general orientation of the two molecules relative to the binding pocket is the same in both cases (Fig. 4b). In this position, pyrrole rings C and D of *N*-MeMP are essentially superimposed on rings A and B of dSDP This planarity of the bound dSDP clearly suggests that a prerequisite to macrocycle distortion is its insertion into the binding pocket of the enzyme.

Discussion

The recently determined structures of the Glu343Lys variant of human ferrochelatase in complex with the substrate ppIX, of the lead-inhibited intermediate of the wild-type enzyme, and of the product complex of the Phe110Ala variant show that the porphyrin is bound in an orientation that is different from that observed in the structures of the *B. subtilis* enzyme. In human ferrochelatase, the porphyrin is rotated by about 100° and buried by an additional 4.5 Å deeper into the active site cleft, relative to the position of N-MeMP bound to the *B. subtilis* enzyme.[22,23] The structures of the human enzyme also show that the porphyrin binding cleft is in a closed conformation as compared to the porphyrin-free protein, whereas in *B. subtilis* ferrochelatase the entrance to the cleft is more open after porphyrin binding. Based on these results, it has been suggested that the mode of binding of *N*-MeMP to *B. subtilis* ferrochelatase may not reflect the proper substrate-binding mode.[22] However, our observation that *N*-MeMP bound to wild-type *B. subtilis* ferrochelatase could be metallated while in the complex with the His183Ala variant it could not, suggests strongly that the porphyrin is bound to the protein in a “productive” state.

The differences in porphyrin binding and cleft conformation found in *B. subtilis* and human ferrochelatase structures may be explained by factors other than improper binding of the inhibitor. Thus, as shown in Fig. 5a, the porphyrin-binding clefts in the two subunits of *S. cerevisiae* ferrochelatase have different conformations—one of which is open and similar to the conformation of the porphyrin-free human ferrochelatase, while the other is closed and is similar to the conformation of human ferrochelatase in complex with porphyrin. This suggests that both variants of the structure, the closed and the open, may co-exist in solution and that porphyrin binding just stabilizes the closed conformation. In the case of the porphyrin-free structure of the human enzyme, several detergent molecules bound at the entrance to the cleft seem to stabilize the open conformation of both monomers.[22] In addition, comparison of the

structures of human, yeast, *B. subtilis* and *B. anthracis* (PDB code 2C8J) ferrochelatase shows marked differences between the bacterial and eukaryotic enzymes around the entrance to the active site pocket. This is shown in Fig. 5b and c, where the structure of the *N*-MeMP complex of the *B. subtilis* enzyme is superimposed on the two monomers of the *S. cerevisiae* enzyme (PDB codes 1C1H and 1LBQ, respectively). The superposition shows that while helix 1 and the loop between helices 1 and 2 are of approximately the same length in the eukaryotic and bacterial enzymes, helix 2 is longer in the yeast enzyme (residues Thr78–Gly99 and Glu38–Gly51 in yeast and *B. subtilis* ferrochelatase, respectively). There is also a kink caused by Pro89 in the middle of the helix in the yeast structure. The figures show that binding of the porphyrin to the closed conformation of the yeast (or human) ferrochelatase in the same orientation as in the *B. subtilis* enzyme will result in a steric clash with main-chain and side-chain atoms from helix 2 in the closed conformation of the protein. Thus, porphyrin binding to the human and yeast ferrochelatase, and presumably other eukaryotic ferrochelatases, in the same orientation as in *B. subtilis*, would not allow closure of the cleft. This suggests the exciting possibility that bacterial and eukaryotic ferrochelatase may bind the porphyrin in two different orientations and still achieve the same type of distortion required for metal insertion.

The structures of ferrochelatase with *N*-MeMP show clearly that only one isomer out of 8 is bound to the enzyme. Early studies of ferrochelatase inhibition by different regio-isomers of *N*-alkylated porphyrins are somewhat contradictory and difficult to explain in structural terms. Thus, in 1980 Ortiz de Montellano *et al.*[38] found that the four regio-isomers of *N*-MePP inhibited ferrochelatase with equal potency. On the other hand, De Matteis *et al.*[39] showed that *N*-MeMP fractions N_C+N_D are more potent inhibitors than N_A+N_B, but for the Zn-complexes of *N*-MeMP and *N*-MePP fractions, N_A+ N_B are more potent than N_C+N_D. In the case of *N*-ethylprotoporphyrin IX, enantiomers (*R*)-N_A and (*S*)-N_B were the most potent inhibitors,[40] while alkylation of rings C and D resulted in only weak inhibition of ferrochelatase activity.[39,41] It cannot be excluded that during crystallization complexes with different regio-isomers exist in solution, but the crystallization process favors only one of the regio-isomers. However, the suitability of a certain complex for crystallization normally suggests that this complex is the most stable. In addition, the complex of the His183Ala variant of ferrochelatase with regio-isomer N_B of *N*-MeMP clearly shows that the binding pocket has a defined structural preference. It also shows that His183 is essential for the control of the regio-specificity and degree of distortion of the porphyrin. It should be noted that the degree of porphyrin deformation observed for the complexes with ferrochelatase is not unusual. For example, the heme groups of peroxidases exhibit strong saddling (−0.6 to −0.9 Å) and ruffling (−0.3 to −0.7 Å), while in mitochondrial cytochrome *c*, which has a covalently attached heme group, the heme group exhibits large ruffling (0.7–1.0Å) and minor saddling deformations.[36] The analysis also demonstrated that the degree of distortion is highly conserved within a protein family. The conservation of the residues in the binding pocket of ferrochelatase clearly suggests that the type and degree of substrate distortion are also conserved in this case. Another active site residue recently suggested by Shi *et al.*[14] to affect the regio-specificity of porphyrin binding is Pro255 (Pro229 in *B. subtilis* ferrochelatase). This residue is located in the loop that in *B. subtilis* ferrochelatase interacts directly with the porphyrin through Trp230. The replacement of Pro255 by any other residue may affect the conformation of the loop, which will in turn affect porphyrin distortion.

As mentioned earlier, the amino acid residues corresponding to the invariant His183 in other ferrochelatases has been implicated in metal binding, proton extraction and interactions with the porphyrin.[27–32] However, due to the low turnover rate of the ferrochelatase reaction (k_{cat} around 0.1 s^{-1} in the steady state)[42] and the exposure of the bound porphyrin to solvent, extraction of the proton from the macrocycle could be performed directly by solvent instead of an amino acid side chain. The present study clearly confirms that the primary function of His183, in addition to porphyrin distortion, is metal binding and insertion into the macrocycle.

It should also be noted that distortion of the macrocycle may be one of the factors which facilitate proton abstraction, which suggests that His183 indirectly may also contributes to proton abstraction.

The mode of ferrochelatase inhibition by 2,4-di-substituted porphyrins with bulky groups was not known previously. As inferred from the structures of the complexes presented, the two porphyrin compounds inhibit the enzyme in different ways. Although bound in the same orientation, the bulky sulphonic groups of dSDP prevent it from accessing the lower part of the binding cleft, resulting in a location of the macrocycle that is much closer to the surface of the protein. This mode of binding explains the lower inhibition potency of this class of compounds.

Materials and Methods

Preparation of protein and crystallization of *B. subtilis* ferrochelatase

B. subtilis ferrochelatase, expressed in *Escherichia coli* BL21 (DE3) as inclusion bodies, was refolded and purified as described.[43] Site-directed mutagenesis was previously performed to construct the plasmid encoding the His183Ala variant of *B. subtilis* ferrochelatase.[32] Crystals of the His183Ala ferrochelatase complexed with *N*-MeMP (Frontier Scientific, Logan, UT, USA) were initially grown by vapor diffusion,[20] and subsequently optimized by seeding techniques. For metal soaking, crystals were transferred to a drop containing well solution (see below) and 5 mM $CuSO_4$, and soaked for either 30 min or 120 min. Crystals of ferrochelatase in complex with dSDP (Frontier Scientific, Logan, UT, USA) were generated in a similar way, the well solution being composed of 30% PEG 2000, 0.2 M $MgCl_2$ and 0.1 M Tris–HCl, pH 8.0. The drop contained glycine, which was required as an additive, at a final concentration of 0.1 M.

Fluorescence titration measurements

The binding of dSDP to wild-type and His183Ala variant ferrochelatases were estimated using fluorescence titration as described for *N*-MePP binding to murine ferrochelatase.[26] The emission at 347 nm from 0.20 μM ferrochelatase excited at 288 nm was monitored as the concentration of dSDP was increased, using a Fluoro-Max-2 fluorimeter (Jobon Yvon Spex). Measurements were carried out on triplicate samples for each condition and enzyme. The k_d values were estimated from the decrease in fluorescence using the software GraphPad Prism‡.

Data collection and refinement

For collection of diffraction data, the crystals were first transferred to a drop containing well solution and 10% PEG 400 as a cryoprotectant. A nylon loop was used to mount the crystal, which was flash-frozen in a stream of boiled-off nitrogen. Data were collected at beamline I911-5 at the MAX II synchrotron radiation facility in Lund, Sweden.[44,45] All data collected were indexed and integrated with the XDS package.[46] Molecular replacement was employed to obtain initial phases using the previously solved crystal structure of *B. subtilis* ferrochelatase with bound *N*-MeMP (PDB code 1C1H) and MOLREP software.[47] The structures were refined using CNS,48 and the models were built using the graphics programs O49 and Coot.50 Statistics for the collected data and quality criteria for the refined structures are given in Table 1.

‡http://www.graphpad.com/prism/Prism.htm

Protein Data Bank accession codes

Coordinates have been deposited with the Protein Data Bank with accession codes 2Q3J and 2Q2N.

Acknowledgments

This work was supported by grants from the Crafoord Foundation to M.H. and by the Swedish Research Council (Vetenskapsrådet) to M.H. and S.A.K. The work of GCF was supported by grants from the National Institutes of Health (GM080270) and the American Heart Association, Florida Affiliate (0655091B).

Abbreviations used

ppIX	protoporphyrin IX
RR	resonance Raman
N-MeMP	*N*-methylmesoporphyrin IX
dSDP	deuteroporphyrin IX 2,4-disulfonic acid dihydrochloride
N-MePP	*N*-methylprotoporphyrin IX
NSD	normal-coordinate structural decomposition

References

1. Fraústo da Silva, RJJ.; Williams, RJP. The Biological Chemistry of the Elements. Vol. 2. Oxford University Press; Oxford, UK: 2001. Haem iron: coupled redox reactions; p. 370-399.
2. Dailey, HA.; Dailey, TA. Ferrochelatase. In: Kadish, KM.; Smith, KM.; Guilard, R., editors. Porphyrin Handbook: The Iron and Cobalt Pigments: Biosynthesis, Structure and Degradation. Vol. 12. Academic Press; San Diego, CA: 2003. p. 93-122.
3. Al-Karadaghi S, Franco R, Hansson M, Shelnutt JA, Isaya G, Ferreira GC. Chelatases: distort to select? Trends Biochem Sci 2006;31:135–142. [PubMed: 16469498]
4. Willows, RD.; Hansson, M. Mechanism, structure, and regulation of magnesium chelatase. In: Kadish, KM.; Smith, KM.; Guilard, R., editors. Porphyrin Handbook: Chlorophylls and Bilins: Biosynthesis, Synthesis and Degradation. Vol. 13. Academic Press; San Diego, CA: 2003. p. 1-47.
5. Schubert HL, Raux E, Wilson KS, Warren MJ. Common chelatase design in the branched tetrapyrrole pathways of heme and anaerobic cobalamin synthesis. Biochemistry 1999;38:10660–10669. [PubMed: 10451360]
6. Hambright P, Chock PB. Metal-porphyrin interactions. 3. A dissociative-interchange mechanism for metal ion incorporation into porphyrin molecules. J Am Chem Soc 1974;96:3123–3131. [PubMed: 4833462]
7. Lavallee, DK. Molecular Structure and Energetics. VCH; Weinheim: 1988. Porphyrin metalation reactions in biochemistry; p. 279-314.
8. Yoon T, Cowan JA. Frataxin-mediated iron delivery to ferrochelatase in the final step of heme biosynthesis. J Biol Chem 2004;279:25943–25946. [PubMed: 15123683]
9. Lesuisse E, Santos R, Matzanke BF, Knight SA, Camadro JM, Dancis A. Iron use for haeme synthesis is under control of the yeast frataxin homologue (Yfh1). Hum Mol Genet 2003;12:879–889. [PubMed: 12668611]
10. O'Neill HA, Gakh O, Park S, Cui J, Mooney SM, Sampson M, et al. Assembly of human frataxin is a mechanism for detoxifying redox-active iron. Biochemistry 2005;44:537–545. [PubMed: 15641778]
11. Karlberg T, Schagerlof U, Gakh O, Park S, Ryde U, Lindahl M, et al. The structures of frataxin oligomers reveal the mechanism for the delivery and detoxification of iron. Structure 2006;14:1535–1546. [PubMed: 17027502]

12. Franco R, Ma JG, Lu Y, Ferreira GC, Shelnutt JA. Porphyrin interactions with wild-type and mutant mouse ferrochelatase. Biochemistry 2000;39:2517–2529. [PubMed: 10704201]
13. Lu Y, Sousa A, Franco R, Mangravita A, Ferreira GC, Moura I, Shelnutt JA. Binding of protoporphyrin IX and metal derivatives to the active site of wild-type mouse ferrochelatase at low porphyrin-to-protein ratios. Biochemistry 2002;41:8253–8262. [PubMed: 12081474]
14. Shi Z, Franco R, Haddad R, Shelnutt JA, Ferreira GC. The conserved active-site loop residues of ferrochelatase induce porphyrin conformational changes necessary for catalysis. Biochemistry 2006;45:2904–2912. [PubMed: 16503645]
15. Blackwood ME, Rush ITS, Romesberg F, Schultz PG, Spiro TG. Alternative modes of substrate distortion in enzyme and antibody catalyzed ferrochelation reactions. Biochemistry 1998;37:779–782. [PubMed: 9457047]
16. Venkateshrao S, Yin J, Jarzecki AA, Schultz PG, Spiro TG. Porphyrin distortion during affinity maturation of a ferrochelatase antibody, monitored by resonance Raman spectroscopy. J Am Chem Soc 2004;126:16361–16367. [PubMed: 15600337]
17. Al-Karadaghi S, Hansson M, Nikonov S, Jönsson B, Hederstedt L. Crystal structure of ferrochelatase: the terminal enzyme in heme biosynthesis. Structure 1997;5:1501–1510. [PubMed: 9384565]
18. Wu CK, Dailey HA, Rose JP, Burden A, Sellers VM, Wang BC. The 2.0 Å structure of human ferrochelatase, the terminal enzyme of heme biosynthesis. Nature Struct Biol 2001;8:156–160. [PubMed: 11175906]
19. Karlberg T, Lecerof D, Gora M, Silvegren G, Labbe-Bois R, Hansson M, Al-Karadaghi S. Metal binding to *Saccharomyces cerevisiae* ferrochelatase. Biochemistry 2002;41:13499–13506. [PubMed: 12427010]
20. Lecerof D, Fodje M, Hansson A, Hansson M, Al-Karadaghi S. Structural and mechanistic basis of porphyrin metallation by ferrochelatase. J Mol Biol 2000;297:221–232. [PubMed: 10704318]
21. Yin J, Andryski SE, Beuscher AE, Stevens RC, Schultz PG. Structural evidence for substrate strain in antibody catalysis. Proc Natl Acad Sci USA 2003;100:856–861. [PubMed: 12552112]
22. Medlock A, Swartz L, Dailey TA, Dailey HA, Lanzilotta WN. Substrate interactions with human ferrochelatase. Proc Natl Acad Sci USA 2007;104:1789–1793. [PubMed: 17261801]
23. Medlock AE, Dailey TA, Ross TA, Dailey HA, Lanzilotta WN. A π-helix switch selective for porphyrin deprotonation and product release in human ferrochelatase. J Mol Biol 2007;373:1006–1016. [PubMed: 17884090]
24. Dailey HA, Fleming JE. Bovine ferrochelatase. Kinetic analysis of inhibition by N-methylprotoporphyrin, manganese, and heme. J Biol Chem 1983;258:11453–11459. [PubMed: 6688622]
25. Dailey HA, Jones CS, Karr SW. Interaction of free porphyrins and metalloporphyrins with mouse ferrochelatase. A model for the active site of ferrochelatase. Biochim Biophys Acta 1989;999:7–11. [PubMed: 2804139]
26. Shi Z, Ferreira GC. Modulation of inhibition of ferrochelatase by *N*-methylprotoporphyrin. Biochem J 2006;399:21–28. [PubMed: 16792525]
27. Kohno H, Okuda M, Furukawa T, Tokunaga R, Taketani S. Site-directed mutagenesis of human ferrochelatase - Identification of histidine-263 as a binding-site for metal-ions. Biochim Biophys Acta 1994;1209:95–100. [PubMed: 7947988]
28. Gora M, Grzybowska E, Rytka J, Labbe-Bois R. Probing the active-site residues in *Saccharomyces cerevisiae* ferrochelatase by directed mutagenesis. *In vivo* and *in vitro* analyses. J Biol Chem 1996;271:11810–11816. [PubMed: 8662602]
29. Sellers VM, Wu CK, Dailey TA, Dailey HA. Human ferrochelatase: characterization of substrate-iron binding and proton-abstracting residues. Biochemistry 2001;40:9821–9827. [PubMed: 11502175]
30. Lecerof D, Fodje MN, Leon RA, Olsson U, Hansson A, Sigfridsson E, et al. Metal binding to *Bacillus subtilis* ferrochelatase and interaction between metal sites. J Biol Inorg Chem 2003;8:452–458. [PubMed: 12761666]
31. Shipovskov S, Karlberg T, Fodje M, Hansson MD, Ferreira GC, Hansson M, et al. Metallation of the transition-state inhibitor *N*-methyl mesoporphyrin by ferrochelatase: implications for the catalytic reaction mechanism. J Mol Biol 2005;352:1081–1090. [PubMed: 16140324]

32. Hansson MD, Karlberg T, Rahardja MA, Al-Karadaghi S, Hansson M. Amino acid residues His183 and Glu264 in *Bacillus subtilis* ferrochelatase direct and facilitate the insertion of metal ion into protoporphyrin IX. Biochemistry 2007;46:87–94. [PubMed: 17198378]
33. Barkigia KM, Nurco DJ, Renner MW, Melamed D, Smith KM, Fajer J. Multiconformational surfaces in porphyrins: previews into excited-state landscapes. J Phys Chem 1998;102:322–326.
34. Shelnutt JA, Song XZ, Ma JG, Jia SL, Jentzen W, Medforth CJ. Nonplanar porphyrins and their significance in proteins. Chem Soc Rev 1998;27:31–41.
35. Jarzecki AA, Spiro TG. Porphyrin distortion from resonance Raman intensities of out-of-plane modes: computation and modeling of *N*-methylmesoporphyrin, a ferrochelatase transition state analog. J Phys Chem A 2005;109:421–430. [PubMed: 16833362]
36. Jentzen W, Ma JG, Shelnutt JA. Conservation of the conformation of the porphyrin macrocycle in hemoproteins. Biophys J 1998;74:753–763. [PubMed: 9533688]
37. Dailey HA, Smith A. Differential interaction of porphyrins used in photoradiation therapy with ferrochelatase. Biochem J 1984;223:441–445. [PubMed: 6497856]
38. Ortiz de Montellano PR, Kunze KL, Cole SP, Marks GS. Inhibition of hepatic ferrochelatase by the four isomers of *N*-methylprotoporphyrin IX. Biochem Biophys Res Commun 1980;97:1436–1442. [PubMed: 6894236]
39. de Matteis F, Gibbs AH, Harvey C. Studies on the inhibition of ferrochelatase by *N*-alkylated dicarboxylic porphyrins. Steric factors involved and evidence that the inhibition is reversible. Biochem J 1985;226:537–544. [PubMed: 3838893]
40. Kimmett SM, Whitney RA, Marks GS. Evidence for the stereoselective inhibition of chick embryo hepatic ferrochelatase by *N*-alkylated porphyrins. II. Mol Pharmacol 1992;42:307–310. [PubMed: 1513328]
41. Ortiz de Montellano PR, Kunze KL, Cole SP, Marks GS. Differential inhibition of hepatic ferrochelatase by the isomers of *N*-ethylprotoporphyrin IX. Biochem Biophys Res Commun 1981;103:581–586. [PubMed: 7332558]
42. Hoggins M, Dailey HA, Hunter CN, Reid JD. Direct measurement of metal ion chelation in the active site of human ferrochelatase. Biochemistry 2007;46:8121–8127. [PubMed: 17566985]
43. Hansson MD, Lindstam M, Hansson M. Crosstalk between metal ions in *Bacillus subtilis* ferrochelatase. J Biol Inorg Chem 2006;11:325–333. [PubMed: 16453119]
44. Mammen CB, Ursby T, Thunnissen M, Als-Nielsen J. Bent diamond crystals and multilayer based optics at the new 5-station protein crystallography beamline ‘Cassiopeia’ at MAX-lab. AIP Conf Proc 2004;705:808–811.
45. Ursby T, Mammen CB, Cerenius Y, Svensson C, Sommarin B, Fodje MN, et al. The new macromolecular crystallography stations at MAX-lab: The MAD station. AIP Conf Proc 2004;705:1241–1246.
46. Kabsch W. Automatic processing of rotation diffraction data from crystals of initially unknown symmetry and cell constants. J Appl Crystallogr 1993;26:795–800.
47. Vagin A, Teplyakov A. MOLREP: an automated program for molecular replacement. J Appl Crystallogr 1997;30:1022–1025.
48. Brunger AT, Adams PD, Clore GM, Delano WL, Gros P, Grosse-Kunstleve RW, et al. Crystallography & NMR system: a new software suite for macromolecular structure determination. Acta Crystallogr D 1998;54:905–921. [PubMed: 9757107]
49. Jones TA, Zou JY, Cowan SW, Kjeldgaard M. Improved methods for building protein models in electron-density maps and the location of errors in these models. Acta Crystallogr A 1991;47:110–119. [PubMed: 2025413]
50. Emsley P, Cowtan K. Coot: model-building tools for molecular graphics. Acta Crystallogr D 2004;60:2126–2132. [PubMed: 15572765]

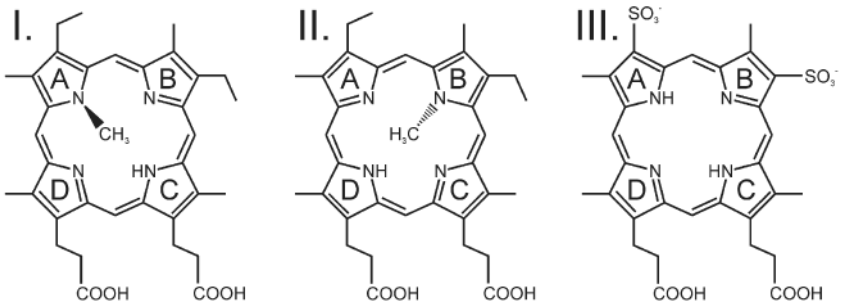

Fig. 1.

A representation of deuteroporphyrin IX 2,4-disulfonic acid dihydrochloride (dSDP) and the *N*-methylmesoporphyrin (*N*-MeMP) isomer structures. (**I**) The (*R*)-enantiomer of N_A, which was bound to wild-type *B. subtilis* ferrochelatase. (**II**) The (*S*)-enantiomer of N_B, which was bound to the His183Ala variant. (**III**) dSDP.

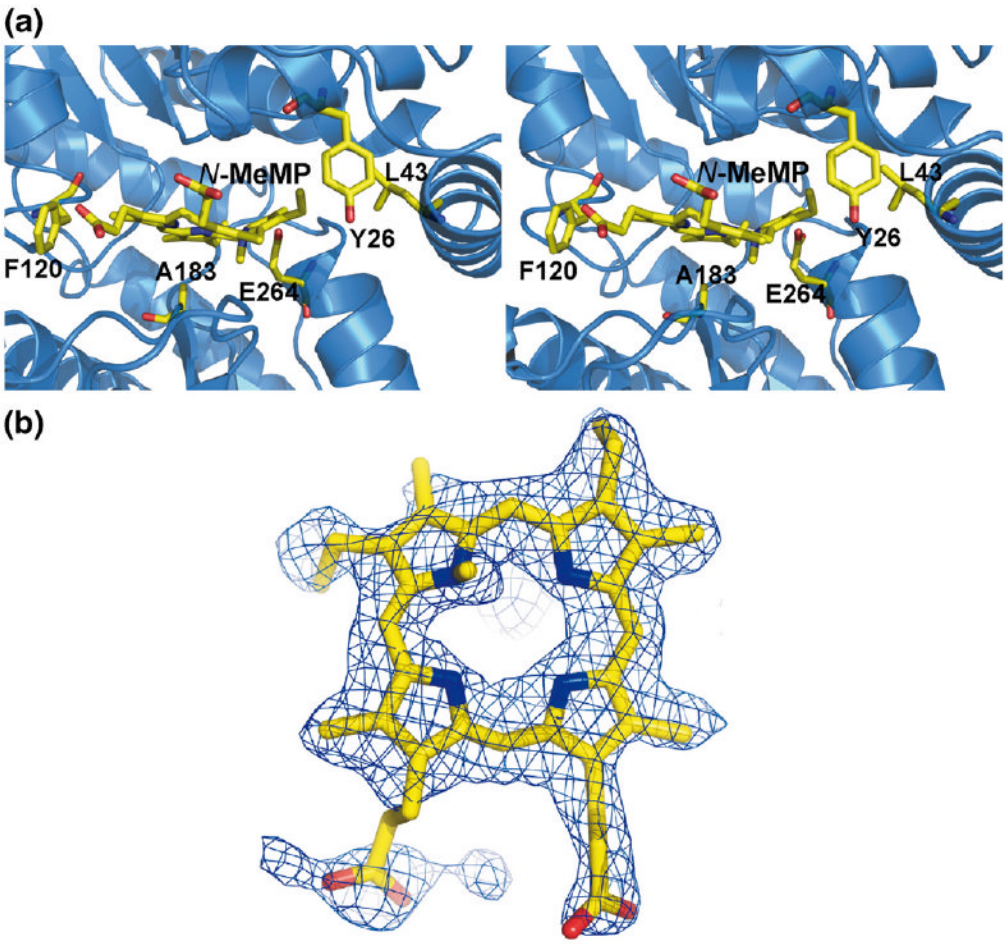

Fig. 2.

Binding of *N*-MeMP to the His183Ala variant of ferrochelatase. (a) A stereo view showing *N*-MeMP regio-isomer N_B in the active site of the His183Ala variant ferrochelatase. (b) The electron density of *N*-MeMP calculated with coefficients ($3F_{obs}-2F_{calc}$) superimposed on the structure of the inhibitor. All figures were prepared using PyMOL [http://pymol.sourceforge.net/].

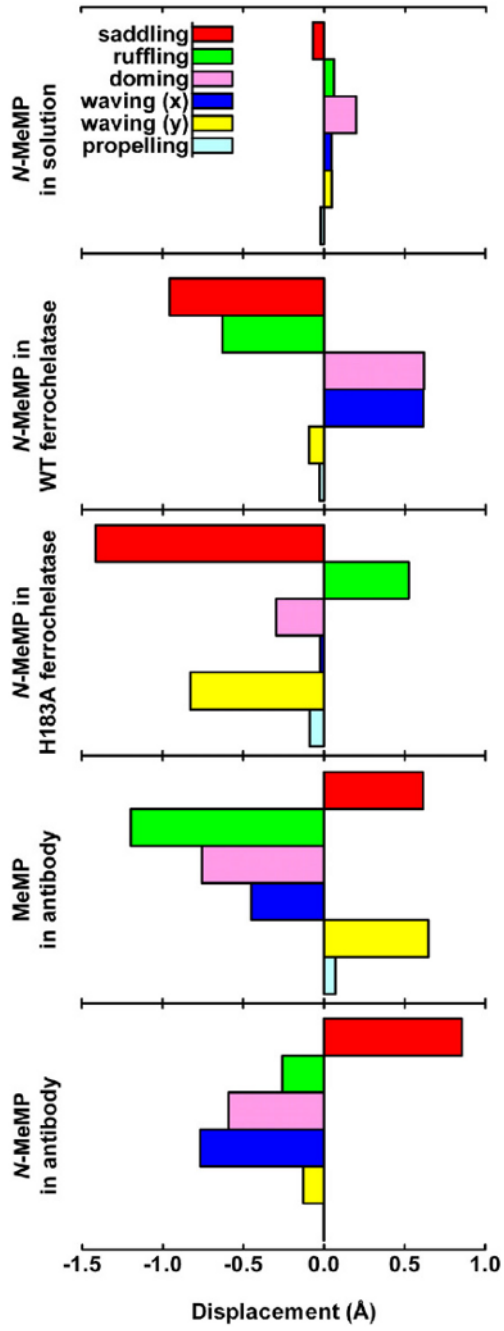

Fig. 3.

NSD of the X-ray crystallographic structures of *N*-MeMP and mesoporphyrin bound to ferrochelatase and a catalytic antibody. Distortion of *N*-MeMP in solution is shown for comparison.

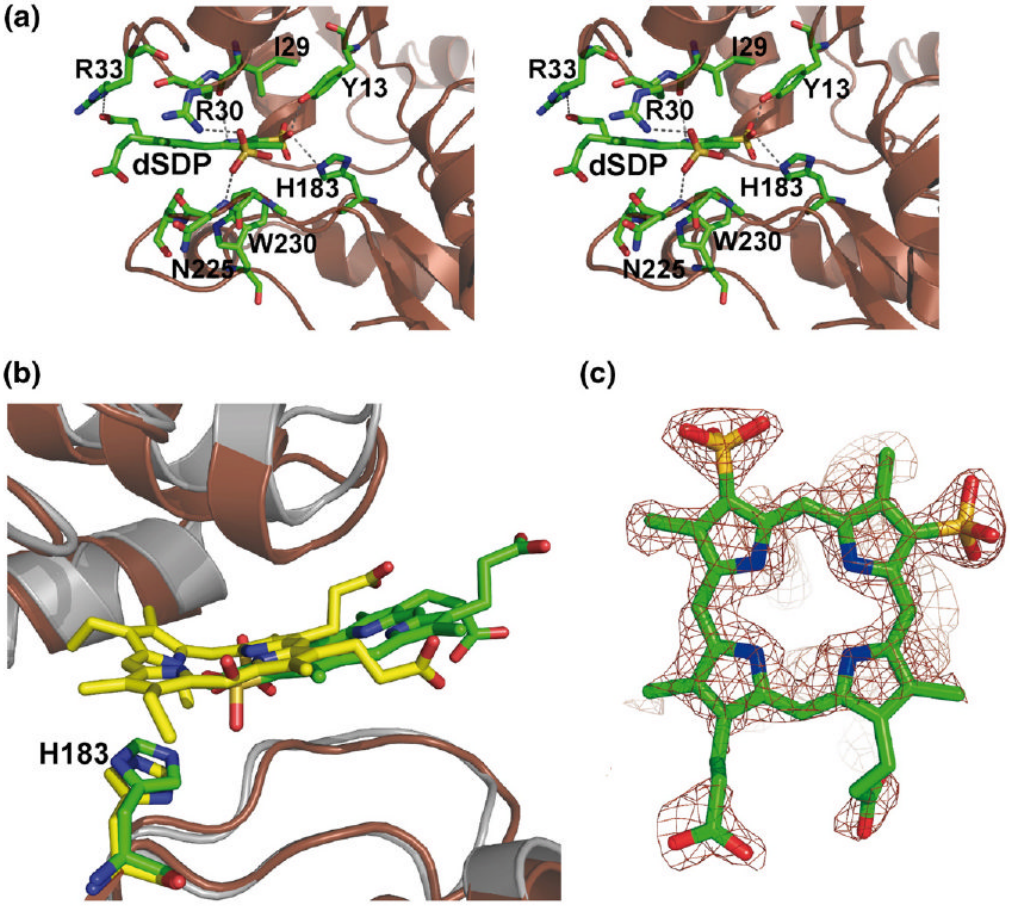

Fig. 4.

Binding of dSDP to wild-type ferrochelatase. (a) A stereo view showing the interactions of dSDP with ferrochelatase. (b) Superposition of the structures of ferrochelatase in complex with *N*-MeMP (yellow) and dSDP (green), showing the relative position of the two inhibitors within the porphyrin-binding cleft. (c) The electron density of dSDP calculated with coefficients ($3F_{obs}-2F_{calc}$) superimposed on the structure of the inhibitors.

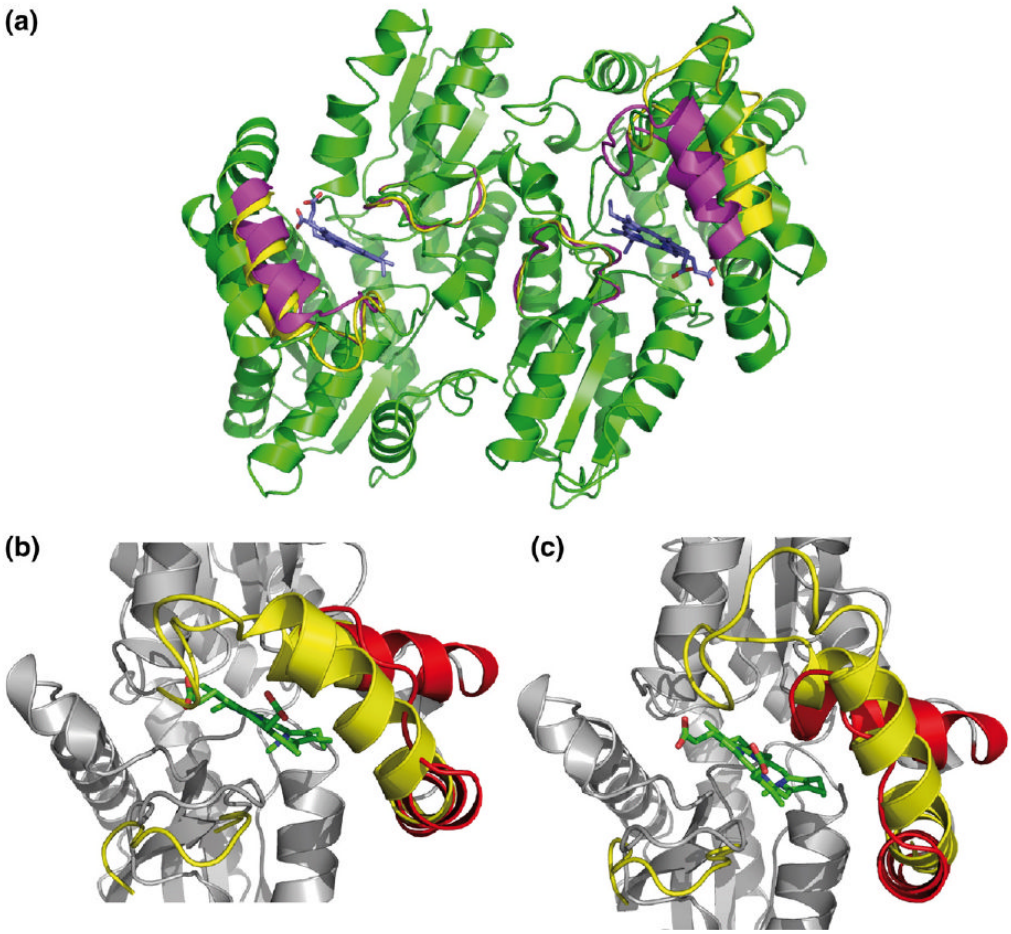

Fig. 5.

Comparison of ferrochelatase structures. (a) Superposition of the *S. cerevisiae* ferrochelatase structure (in yellow; PDB code 1LBQ) on the porphyrin-free (green; PDB code 2HRC) and porphyrin complex (magenta; PDB code 2HRE) of Arg115Leu and Glu343Lys variants, respectively, of human ferrochelatase. The porphyrin molecule (blue) is shown with sticks. (b and c) Superposition of the *B. subtilis* ferrochelatase structure in complex with *N*-MeMP (in gray, with helices 1 and 2 highlighted in red; PDB code 1C1H) on the yeast ferrochelatase monomers with closed (b) and open (c) conformations. *N*-MeMP (green) is shown with sticks. The steric clash of the propionic acid side-chains of *N*-MeMP with the protein structure is visible in b.

Table 1

Statistics for the collected data and quality parameters for the refined structures of His183Ala ferrochelatase co-crystallised with *N*-MeMP and for wild-type enzyme co-crystallised with dSDP

	His183Ala:*N*-MeMP	**Wild-type ferrochelatase:dSDP**
Beamline	I911-5	I911-3
Wavelength (Å)	0.90590	1.00030
Cell dimensions[a] (Å)		
a	49.8	48.4
b	58.6	49.9
c	97.8	118.4
Resolution range (Å)	20.0–2.4	30–1.8
Completeness (%)	97.9	94.1
No. unique reflections	11,648	25,719
Multiplicity	5.1	8.1
$I/\sigma(I)>3$ (%)	91.3	94.1
R_{merge}[b] (%)	7.5	8.7
In the highest-resolution shell Resolution range (Å)	2.5–2.4	2.0–1.8
Completeness (%)	92.3	96.4
$I/\sigma(I)>3$ (%)	81.4	96.4
R_{merge} (%)[b]	18.1	37.0
Refinement		
No. protein atoms	2455	2493
No. water molecules	140	257
R_{cryst} (R_{free})[c] (%)	18.3 (22.8)	19.2(25.0)
Mean *B*-value (Å^2)	24.2	25.1
r.m.s.d.[d]		
Bond lengths (Å)	0.006	0.012
Bond angles (deg)	1.3	1.5
PDB code	2Q3J	2Q2N

[a] Space group $P2_12_12_1$.

[b] $R_{merge}=\Sigma|I_i-<I>|/\Sigma I$, where I_i is an individual intensity measurement and $<I>$ is the average intensity for this reflection.

[c] $R_{cryst}=\Sigma|F_{obs}-F_{calc}|/\Sigma F_{obs}$, where F_{obs} and F_{calc} are the ob served and calculated structure factor amplitudes, respectively. R_{free} is the same as R_{cryst} but calculated on 5% of the data excluded from refinement.

[d] Root-mean-square deviations (r.m.s.d.) of the parameters from their ideal values.